

Numerical fluid flow modelling and its seismic response in time-lapse

Vanja Milicevic and Dr. Robert J. Ferguson

ABSTRACT

A timelapse reservoir characterization study is performed on a model of a producing reservoir. This model reservoir has two injection wells and one producer. Pressure and saturation models are obtained from numerical simulation of reservoir properties and fluid flow for a number of calendar days. Integration of saturation models and Gassmann's relations delivers compressional wave velocity models for each calendar day, and finite-difference algorithms are used to generate synthetic data for comparison; specifically, we compare 2D acoustic and 3C-3D elastic forward modelling. Examples show subtle similarities and differences between the models. Both, acoustic and elastic, models prove to be valuable tools in reservoir characterization.

INTRODUCTION

Development of a reservoir depends on the alliance of geologists, geophysicists and engineers. These scientists work closely towards a common goal: reservoir localization, production and characterization under economical means (Hubbard, personal communication). To highlight prospective areas, geologists study the area, define source rocks, reservoir rocks and construct plays (Hubbard, personal communication). Geophysicists acquire and interpret seismic data to obtain subsurface images (Kearey et al., 2002). These images help identify formations, traps, folds and possible hydrocarbon reservoir existence (Shearer, 1999). After completion of wells, engineers collect data that aid in production planning and future developments (Vracar, 2007). Each analysis is a significant measure in reservoir characterization.

When infrastructure is set, production begins. Eventually the primary production recovery becomes uneconomical due to reservoir depletion (Cosse, 1993). At this time artificial recovery methods are employed: injections of water, gas, chemicals or steam in heavy oil reservoirs (Cosse, 1993). Success in enhanced recovery requires reservoir familiarity. This is not difficult for reservoirs with long production history, however, it is a challenging task in reservoirs with short to no production history (Vracar, 2007). Then, numerical modelling of injection flow, a usual secondary recovery mechanism, allows visualization and analysis of reservoir properties (Aarnes et al., 2007).

Our study of time-lapse modelling will offer an improvement to modelling seismic responses in reservoirs under enhanced recovery schemes.

Huang and Lin (2006) develop a method for the use of time-lapse seismic responses in enhanced recovery production optimization employing production history. As mentioned above, this data is rather difficult or not possible to rely upon, when it comes to new fields or wells. The rock physics theoretically captures responses in saturation as injection is applied (Stoffa et al., 2008). As Stoffa et al. (2008) experimentally shows fluid

injection causes seismic response changes. Gasmann's relations tie fluid flow to density saturation, P-wave and S-wave velocities (Mavko et al., 2009). Charkraborty (2007) shows fluid flow changes, using Gasmann's relations, trigger changes in time-lapse seismic responses. Bently and Zou (2003) also show, using Gasmann's equations, sonic and density well logs, fluid substitution maps on seismic response. In this paper, we map fluid flow to seismic response focusing on compressional (P) wave velocity models. We generate and compare events on both acoustic and elastic time-lapse models. Since P-wave velocity is a valuable tool in studying and describing rocks lithologic properties (Ferguson, 1995), the study is intended for reservoir characterization to advance. Potentially, the study's scheme will apply to carbon capture and storage.

The designed time-lapse study follows three stages: 1) flow modelling, 2) rock physics, and 3) seismic modelling. In Table 1, Stage I employs flow modelling using reservoir simulator to calculate pressure and saturation through reservoir properties as in Figure 1a. The simulator employed is a set of MATLAB routines, where main routine is *runq5*, provided by SINTEF ICT. Stage II employs rock physics to calculate density, compressional (P), and shear (S) wave velocities as in Figure 1b. This process is a self-coded *Gassmann* routine in MATLAB. Stage III employs P-wave velocity to generate seismic models, both acoustic and elastic, as in Figure 1c. The commercial software *Tiger*, designed by SINTEF ICT, is used for the above purpose. Both seismic models are generated employing the finite-difference method. 2D models are generated invoking exploding reflectors algorithm in acoustic medium. 3C-3D models are generated using a single shot gatherer in elastic medium.

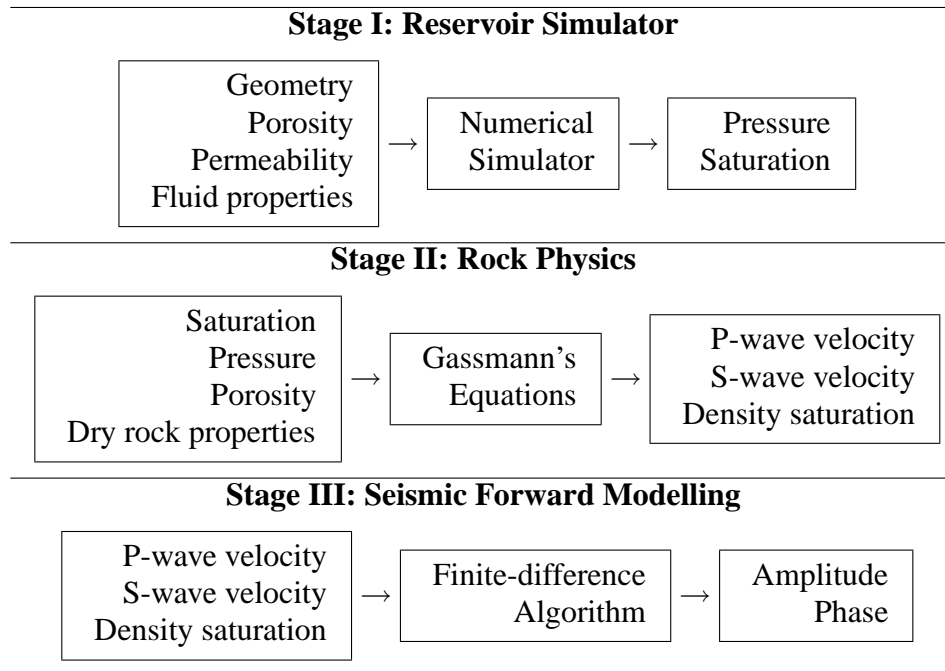


Table 1. Schematic map of preliminary study steps, showing input/output parameters and software used. Stage I shows steps taken to obtain pressure and saturation of the reservoir. Stage II shows the steps taken to calculate density saturation, P-wave and S-wave velocities from saturation. Stage III show the steps taken to generate seismic models from density saturation, P-wave and S-wave velocities.

The acoustic and elastic models are evaluated and compared. Examples show subtle similarities and differences between the models. 2D acoustic show less details than 3C-3D elastic models, however, all major events are identified as strong on both acoustic and elastic models. Both models prove to be valuable tools in reservoir characterization. Its use depends on the study one wishes to exercise.

THEORY

Assume a homogeneous and isotropic reservoir for simulation. The reservoir simulation system consists of two-phase flow, hydrocarbon phase and water phase. Assume 100 % oil saturated sandstone reservoir with one producing and two water injecting wells scenario.

Numerical Fluid Flow

Firstly, assume constant porosity and incompressibility, namely no density variation in time. Also, assume no-flow boundary conditions. In order to model phase flow through porous medium, we start with the continuity equation (Aarnes et al., 2007):

$$\frac{\partial(\phi_p \rho_p)}{\partial t} + \nabla \rho_p v_{f,p} = q_p, \quad (1)$$

where p , ϕ_p , ρ_p , t , $v_{f,p}$ and q_p are desired phase (water or oil), phase density, porosity, time, flow velocity and inflow/outflow per volume, respectively. Now, consider Darcy's law that relates flow velocity, $v_{f,p}$ to pressure, p_p :

$$v_{f,p} = -\frac{k_p}{\mu_p} [\nabla p_p + \rho_p G], \quad (2)$$

where, k_p , μ_p , ρ_p , and G are phase permeability, viscosity, density, and gravitational force, respectively (Aarnes et al., 2007). Now, replacing $v_{f,p}$ in equation (2) with equation (1) we get an elliptic equation for phase pressure conserved in time-lapse (Aarnes et al., 2007):

$$\nabla \cdot v_{f,p} = \frac{q_p}{\rho_p}. \quad (3)$$

Equation (3) describes pressure gradient constant in each grid box over time and its variance from grid box to grid box. The temperature changes are neglected.

$$\phi \frac{\partial s}{\partial t} + \nabla f(s) v_{f,p} = \frac{q_p}{\rho_p}, \quad (4)$$

from the continuity equation of each phase and pore saturation (s), assuming properties of incompressibility and time conservation, that is $s_w + s_o = 1$. Equation (4) estimates saturation from reservoir conditions and water flow in each grid box. The numerical modelling of fundamental reservoir system is done employing equations (3) and (4).

Rock Physics

Gassmann's equations are employed to create velocity models from saturation models. Recall, homogeneous mineral medium and isotropy assumption. Mavko et al. (2009)

states:

$$K_{sat} = K_d + \frac{(1 - \frac{K_d}{K_0})^2}{\frac{\phi}{K_f} + \frac{1-\phi}{K_0} - \frac{K_d}{K_0^2}} \quad \text{and} \quad \mu_{sat} = \mu_d, \quad (5)$$

where ϕ is porosity, and K_{sat} , K_f , K_d , and K_0 are the effective bulk modulus of saturated rock, the effective bulk modulus of pore fluid, the frame bulk modulus of dry rock and the bulk modulus of mineral material making up the rock, respectively. The saturated shear modulus and the dry shear modulus, μ_{sat} , and μ_d , respectively, are independent of saturation (Mavko et al., 2009). Assume constant porosity in the sandstone reservoir. Now, invoke fluid density relation:

$$\rho_f = s_w \rho_w + s_o \rho_o, \quad (6)$$

where ρ_f , s_w , ρ_w , s_o , ρ_o are fluid density, water saturation, water density, oil saturation, oil density, respectively. Using results of equation (6) we obtain density saturation, ρ_{sat} from:

$$\rho_{sat} = (1 - \phi)\rho_0 + \phi\rho_f, \quad (7)$$

where ρ_0 is matrix density. Combination of equation (5) and equation (7) yields P-wave velocity, α (Mavko et al., 2009):

$$\alpha = \sqrt{\frac{K_{sat} + \frac{4}{3}\mu_{sat}}{\rho_{sat}}}, \quad (8)$$

and S-wave velocity, β (Mavko et al., 2009):

$$\beta = \sqrt{\frac{\mu_{sat}}{\rho_{sat}}}. \quad (9)$$

P-wave and S-wave velocity models of the saturated rock are generated using equations (8) and (9), respectively.

Seismic Models

Using the above P-wave and S-wave velocity models, we are able to generate seismic density plots in acoustic and elastic medium employing finite difference algorithm.

The reservoir top and bottom reflections are expected to be stationary on all plots in time-lapse. The waterfronts are anticipated to map sooner as time progresses. Density decrease is expected with water inflow in time. We expect no variation, when laterally correlating density above and below waterfronts in time-lapse. Density above waterfronts alone maps no change in time-lapse.

EXAMPLES

The above developed work flow is applied to the 10th SPE Comparative Solution Project, a free data set publicly available on the internet (Christie and Blunt, 2001) for verification. Data set is also convenient for its capability to run on a single processor. The study comprises of a sandstone reservoir with two injecting and one producing well. The

reservoir has a 3D vertical cross-sectional geometry with no dips or faults (Christie and Blunt, 2001). Its detailed properties are listed in the Table 2. Initially, the reservoir is 100% oil saturated. The reservoir boundaries are impermeable, or no-flow. The viscosity, porosity, and permeability are uniform.

Property	Units
Reservoir	64 x 64 x 1 grid boxes, each grid box: 7.62 m x 7.62 m x 0.762 m
Oil Density	700 kg/m ³
Water Density	1000 kg/m ³
Sandstone Density	2600 kg/m ³
Depth	3900 m
Distance Coverage	3900 m
Initial Pressure (injector)	655 002 Pa
Initial Pressure (producer)	689 476 Pa
Porosity	20 %
Viscosity	1 cp

Table 2. Reservoir properties used in reservoir simulation (Christie and Blunt, 2001).

Numerical Fluid Flow Simulation

A public domain numerical simulator, provided by SINTEF ICT, consists of several MATLAB routines, whose main one is *runq5* (Aarnes et al., 2007). It models reservoir fluid flow. The study models two-phase flow, that is oil production simulation through water injection in 28 days. The study's duration is short due to the stable reservoir conditions and low mobility ratio, that is low oil and water viscosity ratio. The phases are immiscible and incompressible, namely there are no blending or density changes (Cosse, 1993). Water and oil saturations are irreducible, that is oil is fully displaceable by water (Aarnes et al., 2007). The producer is located at the center of the reservoir. The two injectors are situated on the left and right side of the producer at equal distances. Assume symmetry around the producing well, that is area from producer to injector on the right hand side is a mirror image of the reservoir from producer to injector on the left hand side.

The reservoir properties are employed to produce pressure and saturation models. For simplicity of illustration, we only present producer with the injector on the right side.

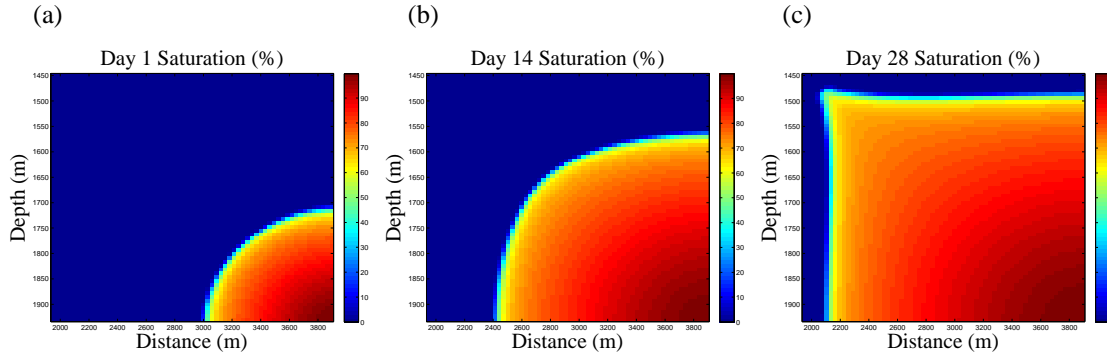


FIG. 1. Reservoir is initially 100% oil saturated. The producer and injector are located in the upper-left and lower-right corner of the model, respectively. The injector pumps water into the reservoir. The profiles 1(a), 1(b) and 1(c) show reservoir as water saturation decreases towards the producer intime-lapse steps after day $\tau = 1, 14, 28$, respectively.

The water injector and oil producer are situated in the upper-left and lower-right corner of the grid in Figure 1, respectively. Figure 1(a) and 1(b) capture water saturation increase and in situ oil displacement after day 1 and day 14, respectively. Figure 1(c) illustrates leading water front after 28 days as it develops finger like flow up to the breakthrough in the production. Note the water injection is constant throughout 28 days.

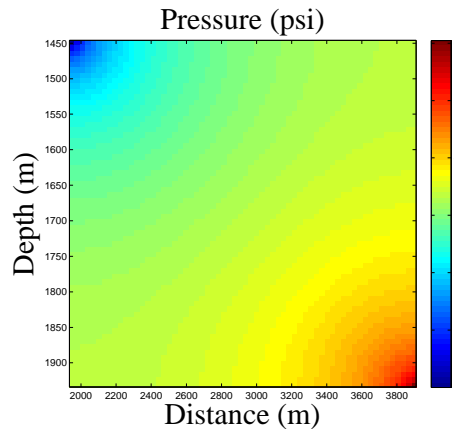


FIG. 2. The initial pore pressure model. The producer and injector are located in the upper-left and lower-right corner of the model, respectively. Pressure decreases from injector to producer. Assume pressure is constant through a 28 dayssimulation.

Figure 2 illustrates initial pressure of the reservoir as it decreases from injector to producer. Assume initial pressure to be constant in each grid box through a 28 day simulation (Aarnes et al., 2007).

Rock Physics

As described in theory section, using saturation models and Gassmann's relations, MATLAB code is designed to calculate density saturation. Assume constant porosity in the reservoir. This assumption yields constant K_d and K_0 precisely listed in Table 3.

Property	Units
Sandstone Shear Modulus	5.04 <i>GPa</i>
Sandstone Bulk Modulus	0.70 <i>GPa</i>
Water Bulk Modulus	2.20 <i>GPa</i>
Oil Bulk Modulus	2600 <i>kg/m³</i>

Table 3. Constants used in Gassmann's equation in obtaining the effective bulk modulus of saturated rocks, K_{sat} (Mavko et al., 2009) and (Beer and Maina, 2008).

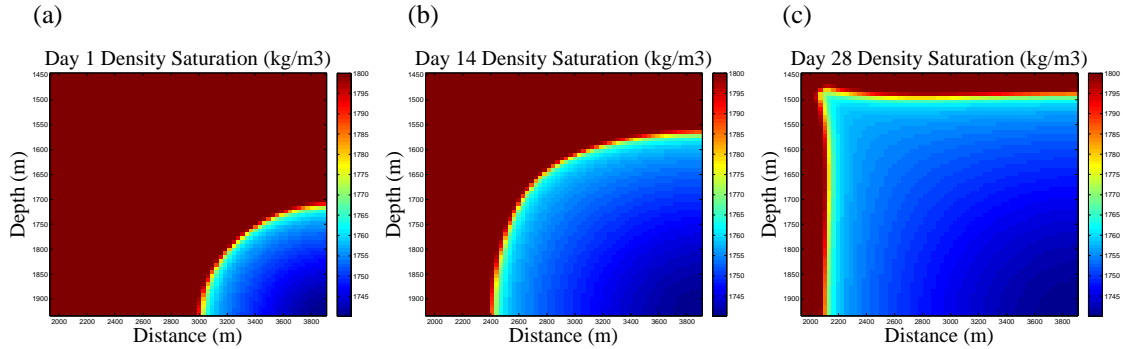


FIG. 3. Density Saturation models. The reservoir is initially 100 % oil saturated. The producer and injector are located in the upper-left and lower-right corner of the model, respectively. The injector pumps water into the reservoir. The models 3(a), 3(b) and 3(c) show reservoir as density saturation increases towards the producer in time-lapse steps after day $\tau = 1, 14, 28$, respectively.

Figure 3(a), 3(b), and 3(c) show density saturation after day 1, 14, and 28, respectively. Note an increase of density from injector to producer. This observation is due to water saturation and density of fluid, as they are directly related to the density of saturated rock. Water saturation increases with injection, and once oil saturated rocks are replaced by water saturation. Water saturated rocks consequently increase the density of fluid and hence the density of saturated rocks.

Further, density saturation motivates velocity models building. Since we assume irreducibility, the bulk modulus of pore fluid is constant. This assumption assures no changes in S-wave velocity, hence we only focus on P-wave velocity models. Also, P-wave velocity is a valuable tool in further studying and describing rocks lithologic properties (Ferguson, 1995) needed in reservoir characterization.

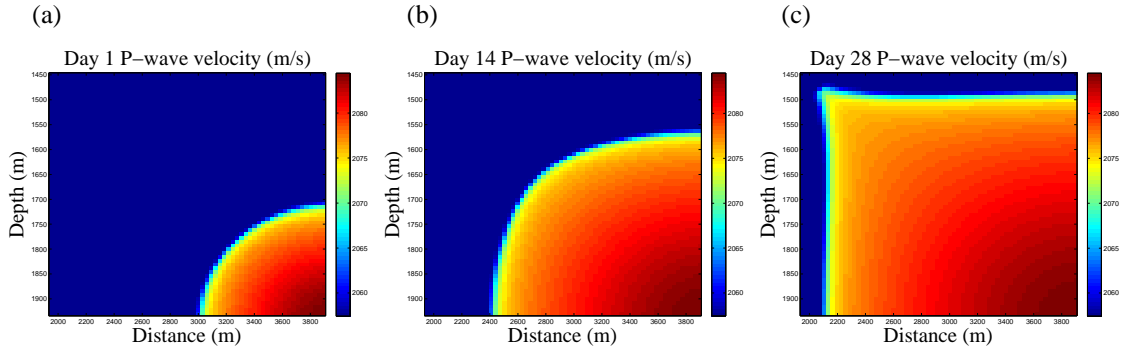


FIG. 4. P-wave velocity calculated from density saturation using Gassmann relations. The reservoir is initially 100 % oil saturated. The producer and injector are located in the upper-left and lower-right corner of the model, respectively. The injector pumps water into the reservoir. The models 4(a), 4(b) and 4(c) show reservoir as P-wave velocity increases towards the producer in time-lapse steps after day $\tau = 1, 14, 28$, respectively.

Empirically, P-wave velocity is greater in water than in oil saturated rocks (Kearey et al., 2002). Figure 4(a), 4(b), and 4(c) illustrate exactly this, P-wave velocity decreases from injector to producer after day 1, 14, and 28, respectively. This occurs because the pressure is higher near the injectors and lower near the producer.

Seismic Modelling

To obtain time-lapse seismic sections the above P-wave velocity model is padded. Linear velocity is applied above the reservoir (Ferguson, personal communication).

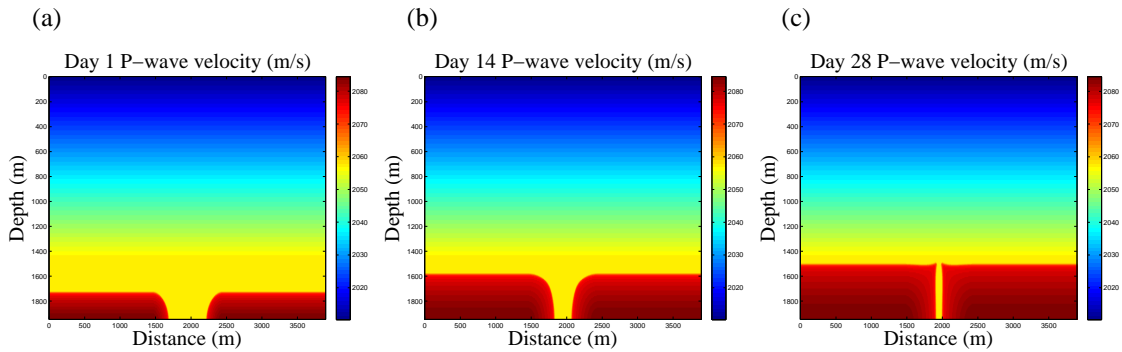


FIG. 5. Padded velocity models used in generating seismic models. The profiles 5(a), 5(b) and 5(c) show reservoir as water saturation increases the P-wave velocity decreases from injector to producer in time-lapse steps after day $\tau = 1, 14, 28$, respectively.

Figure 5(a), 5(b) and 5(c) illustrate padded P-wave velocity models now showing two injectors and one producer scenario after day 1, 14, and 28, respectively. Recall, two injectors are situated in lower left and right corners. One producer is at a half way distance between injectors. Note we still see the same trend in velocity measurements.

Firstly, the above P-wave velocity profiles are used to create 2D exploding reflector seismic gatherers employing function *afd_explode* from the MATLAB CREWES Project

toolbox. The wavefield is propagated in depth using finite difference method, and when convolved with a minimum phase wavelet produces a seismic gather in acoustic medium. As model forces, density saturation set constant. Samples are taken every 4ms.

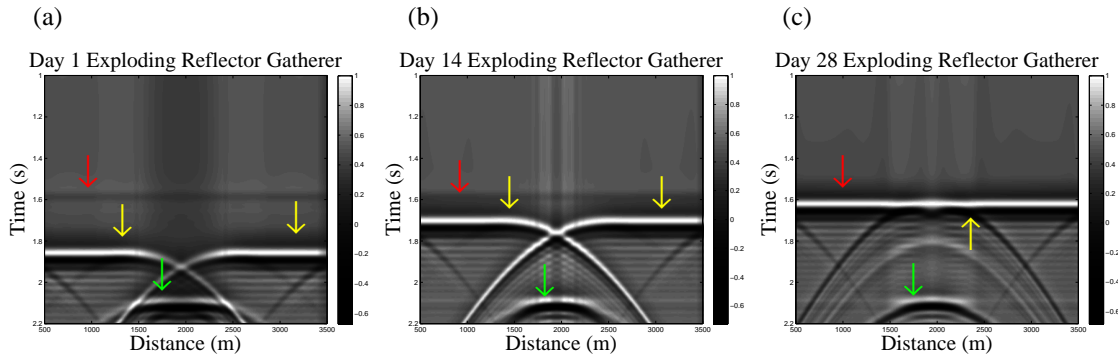


FIG. 6. 2D Exploding Reflector Seismic Gatherer models. The profiles 6(a), 6(b) and 6(c) show reservoir in time-lapse steps after day $\tau = 1, 14, 28$, respectively. The red and green arrows point to the reservoir top and bottom, respectively. The yellow arrows point at the two waterfrofts. Note waterfrofts progress upwards in time-lapse.

Figure 6(a) shows the exploding reflector gatherer after day 1. Observe the top and the bottom of the reservoir at about 1.6s and at about 2.1s, denoted by red and green arrows respectively, that stay stationary until day 28. Both waterfrofts, denoted by yellow arrows, are seen at about 1.85s. Figure 6(b) illustrates seismic after day 14. Note waterfrofts to move up with injection and appear sooner at about 1.7s. Figure 6(c) captures seismic after day 28. Observe a water breakthrough at the producer. The reservoir bottom is pronounced as a strong low followed by a strong high amplitude. The amplitude dims as water saturation increases. The reservoir top is pronounced by a relatively strong and high amplitude. The amplitudes dim as waterfront reaches the producer. Both waterfrofts are captured by low amplitude, observed from sooner to later travelttime arrivals, creating a bow-tie effect. Also, note the reservoir top and bottom and waterfrofts appear in reflection coefficients of opposite polarity. They are positive at the reservoir top and bottom and negative at waterfrofts.

Then, the above 2D P-wave velocity model is extended to a 3D model in MATLAB. This model is used in generating 3C-3D seismic models also employing finite difference algorithm using *Tiger*, commercial software designed by SINTEF ICT. The models are created in elastic medium.

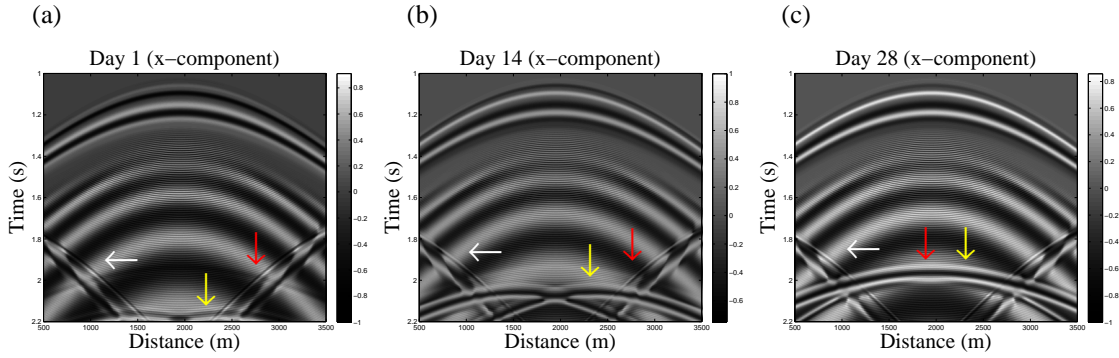


FIG. 7. 3C-3D Shot Gatherer Models: x-component velocity models in elastic medium. The x-component captures shear waves. The red arrow points to the top of the reservoir. The yellow arrow points towards two waterfronfts. The waterfronfts propagate upwards in time-lapse. Both are projections of P-wave velocity onto the shear wave velocity mode. The white arrow marks the reservoir boundary.

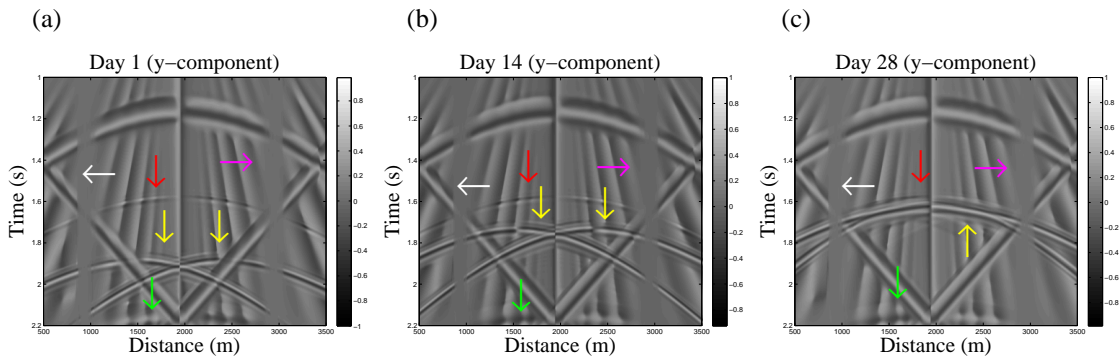


FIG. 8. 3C-3D Shot Gatherer Models: y-component velocity models in elastic medium. The y-component captures converted waves. The red and green arrows point to the top and bottom of the reservoir, respectively. The yellow arrows point towards two waterfronfts. The waterfronfts propagate upwards in time-lapse. The white and magenta arrows mark the reservoir boundary and numerical artifacts, respectively.

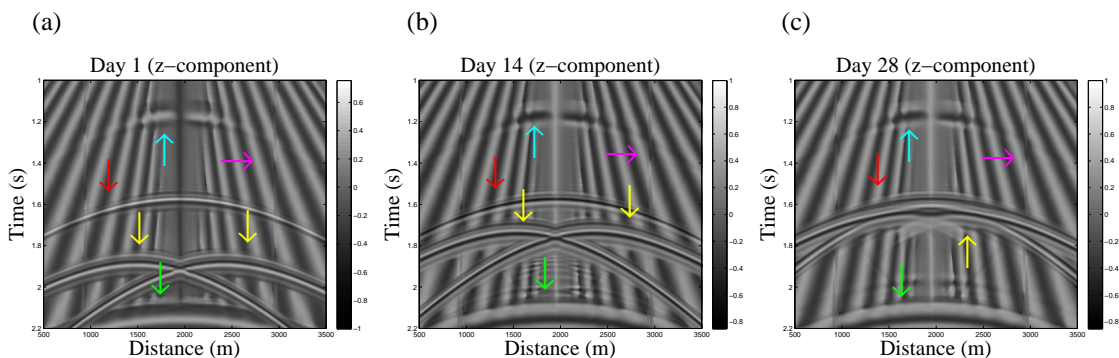


FIG. 9. 3C-3D Shot Gatherer Models: z-component velocity models in elastic medium. The red and green arrows point to the top and bottom of the reservoir, respectively. The yellow arrows point towards two waterfronfts. The waterfronfts on elastic models also progress upwards in time-lapse after day 1, 14 and 28. The 3C-3D models plot more details, hence we see numerical artifacts and projection of shear waves on the the vertical component, pointed by magenta and turquoise arrows, respectively.

Now, observe each component individually. Figures 7(a), 7(b) and 7(c), x-component velocity models, mainly show S-waves. At about 1.8s to about 2.2s reservoir boundaries, denoted by white arrow, appear as slanted linear events. A very weak projection of P-waves from z-component is seen at about 2.0s and at about 2.2s. The two projections are inferred to be reservoir top and waterfronfs, denoted by red and yellow arrows, respectively. Observed in time-lapse waterfronfs progress upwards. Figures 8(a), 8(b) and 8(c), y-component velocity models, capture converted waves, that is P-waves reflected as S-waves. Both reservoir boundaries show at about 1.4 to about 2.2s also as slanted linear events annotated by the white arrow. We note reservoir top and bottom, pointed to by the red and green arrow, at about 1.6s and 2.1s, respectively. Also note the two waterfronfs, pointed to by the yellow arrows, progressing upwards with time. Numerical artifacts, denoted by magenta arrow, are present at about 800m and 3000m on the distance axis. Figures 9(a), 9(b) and 9(c) are z-component velocity models. These models are directly comparable to the acoustic models. The reservoir top and bottom, at about 1.6s and at about 2.1s, respectively, show on 3D elastic models as stationary as well. In Figure 9 the reservoir top and bottom are denoted by red and green arrows, respectively. The reservoir bottom is characterized by a set of high-low-high amplitudes from sooner to later traveltme arrivals. The reservoir top characterized by a set of low-high-low amplitudes, is smeared by a set of high-low-high amplitudes after 28 days. The waterfronfs, denoted by yellow arrows, as in 2D models also create a bow-tie effect. Both waterfronfs show as high amplitudes and progress upwards in time-lapse. The same pattern of reversed polarity between reservoir top and bottom and waterfronfs still applies. Also, note S-wave projection from x-component, marked by the turquoise arrow, at about 1.18s, stationary in time-lapse. Again, numerical artifacts, denoted by magenta arrow, are present at about 800m and 3000m on the distance axis.

The acoustic and elastic medium models reflect the major expected events, such as the two waterfronfs, reservoir top and bottom. We do note more details on the 3C-3D plots. The two approaches both prove to be valuable and its use depends on the reservoir characterization study. The examples prove work flow feasible and expectations verified.

DISCUSSION

The study assumes perfect reservoir conditions, as it is a model of the work flow for Alberta-centric study. In practice, reservoirs are not commonly homogeneous nor 100 % oil saturated. In reality, viscosity, porosity, and permeability are almost never completely uniform. The phases are not immiscible and incompressible, namely there are blending and density changes. Further, water and oil saturations are not fully irreducible, that is oil is not fully displaceable by water. Since the study is a model of work flow, it only lasts 28 days. In the near future, the study will employ channel models and acousto-elstic algorithms. The results will be evaluated in time-lapse steps. Eventually, the work flow will apply to real data set of Balckfoot field in Alberta. This is where numerical artifacts are expected to minimize.

CONCLUSION

A time-lapse study takes place on a reservoir employing one producing and two injecting wells. The study follows three stages: numerical simulation, Gassmann's relations and finite-difference algorithm. The numerical simulation of fluid flow produces saturation and pressure models. Then, the saturation models deliver P-wave velocity models as a result of Gassmann's relations. Further, P-velocity models, through finite-difference algorithms, generate 2D acoustic and 3C-3D elastic seismic models. The theoretical concepts are verified through numerical examples. There are subtle similarities and differences between acoustic and elastic models. Study proves both, acoustic and elastic models, to be assets to reservoir characterization.

REFERENCES

- Aarnes, J. E., Gimse, T., and Lie, K. A., 2007, An introduction to the numerics of flow in porous media using matlab, *in* Hasle, G., Lie, K., and Quak, E., Eds., Numerical Simulation, and Optimization: Applied Mathematics at SINTEF, Springer, 265–306.
- Beer, M. D., and Maina, J. W., 2008, Some fundamental definitions of the elastic parameters for homogeneous isotropic linear elastic materials in pavement design and analysis: the 27th Southern African Transport Conference.
- Bently, R., and Zou, Y., 2003, Time-lapse well log analysis, fluid substitution, and AVO: The Leading Edge, **22**, 550 – 554.
- Charkraborty, S., 2007, An integrated geologic model of valhall oil field for numerical simulation of fluid flow and seismic response: M.Sc. thesis, University of Texas at Austin.
- Christie, M. A., and Blunt, M. J., 2001, Tenth SPE comparative solution project: A comparison of upscaling techniques: SPE Reservoir Engineering and Evaluation, Society of Petroleum Engineers, **4**, 308–317.
- Cosse, R., 1993, Basics of Reservoir Engineering: Oil and Gas Field Development Techniques: Editions TECHNIP.
- Ferguson, R. J., 1995, P-P and P-S inversion of 3-C seismic data: Blackfoot, Alberta: CREWES Research Report, **7**, 41.1–41.12.
- Huang, X., and Lin, Y., 2006, Production optimization using production history and time-lapse seismic data: SEG Expanded Abstracts, **25**, 3145 – 3149.
- Kearey, P., Brooks, M., and Hill, I., 2002, An Introduction to Geophysical Exploration: Blackwell Publishing.
- Mavko, G., Mukerji, T., and Dvorkin, J. I., 2009, The Rock Physics Handbook: Cambridge University Press.
- Shearer, P. M., 1999, Introduction to Seismology: Cambridge University Press.
- Stoffa, P. L., Jin, L., Sen, M. K., and Seif, R. K., 2008, Time-lapse seismic attribute analysis for a water-flooded reservoir: Journal of Geophysics and Engineering, **5**, 210 – 220.

Vracar, B., 2007, Pressure transient analysis, Tech. rep., SAIT.